LHCb Collaboration

LHCB 2003-091
12th August 2003

Photon and Neutral Pion reconstruction

Olivier Deschamps[1]
LPC, Clermond-Ferrand, France

Frederic Machefert[2], **Marie-Helene Schune**[3]
LAL, Orsay, France

Galina Pakhlova[4]
ITEP, Moscow, Russia

Ivan Belyaev[5]
CERN, Geneva, Switzerland
and
ITEP, Moscow, Russia

[1] odescham@in2p3.fr
[2] machefer@in2p3.fr
[3] schunem@lal.in2p3.fr
[4] galya@iris1.itep.ru
[5] Ivan.Belyaev@itep.ru

Abstract

The reconstruction of neutral particles is performed by LHCb calorimeters. The photons are reconstructed from neutral clusters in ECAL which are not associated with reconstructed tracks. For precise determination of photon parameters in addition the information from Prs and Spd detectors are used. Neutral pions are reconstructed either from 2 photons ("resolved" π^0) or from single cluster in ECAL ("merged" π^0). The note describes in detail the reconstruction, energy and position correction techniques and identification procedure for photons, the reconstruction of "resolved" π^0 from pair of photons and the reconstruction of "merged" π^0 from single cluster in ECAL using dedicated iterative techniques.

1 Photon reconstruction

1.1 Clusterisation and cluster processing

Energy deposits in Ecal cells are clusterized with the Cellular Automaton algorithm [3]. According to the clusterisation procedure each local maximum (the calorimeter cell with the energy deposition in excess of the energy deposition in each of its neighbouring cells) originates the cluster. The formal definition of neighbouring cells includes also the cells which touch only in one point[6]. ECAL zero suppression procedure [1] requires the transverse energy of any local maximum to be in excess of 50 MeV[7].

As direct consequence of these formal definitions, the centers of the reconstructed clusters are always separated at least by one cell.

Often one calorimeter cell is shared between several reconstructed clusters. In this case the energy of the cell is redistributed between the clusters proportionally to a total cluster energy. The process is iterative and it converges rapidly due to relatively small ratio of Molier radius to the cell size. The five iterations are enough for convergency.

After the redistribution of energy of shared cells, the first (hypotheses independent) evaluation of global cluster parameters is performed. The cluster energy and position of barycenter are defined as

$$\epsilon = \sum \epsilon_i \qquad x_b = \frac{1}{\epsilon}\sum_i x_i\epsilon_i \qquad y_b = \frac{1}{\epsilon}\sum_i y_i\epsilon_i \tag{1}$$

where ϵ_i, x_i and y_i are cell energy, x- and y-positions of the cell center and the sum runs over all cells in the cluster. The 3×3 covariance matrix for these values is defined using the following parametrisation of covariance matrix for cell energy depositions:

$$\epsilon_i = \mathcal{S}_i^g\ \mathbf{e}_i + \mathcal{G}_i\ \left(\mathcal{N}_i^{in} + \mathcal{N}^{coh}\right) \tag{2}$$

$$\begin{aligned} \mathcal{C}\left\{\epsilon_i, \epsilon_j\right\} &= (i \neq j) \quad \mathcal{G}_i\mathcal{G}_j\mathcal{D}\left\{\mathcal{N}^{coh}\right\} \\ \mathcal{C}\left\{\epsilon_i, \epsilon_i\right\} &= (i = j) \quad \mathcal{D}\left\{\epsilon_i\right\} = \\ &= \mathbf{e}_i^2\mathcal{D}\left\{\mathcal{S}_i^g\right\} + \mathcal{M}^2\left\{\mathcal{S}_i^g\right\}\ \mathcal{D}\left\{\mathbf{e}_i\right\} + \mathcal{G}_i^2\mathcal{D}\left\{\mathcal{N}_i^{in}\right\} + \mathcal{G}_i^2\mathcal{D}\left\{\mathcal{N}^{coh}\right\} \end{aligned} \tag{3}$$

Where $\mathcal{G}_i$,$\mathcal{S}_i^g$ and $\mathcal{N}_i^{in}$ are the gain, the relative gain and the incoherent noise (in ADC channels) for the cell i correspondingly and $\mathcal{N}^{coh}$ is the coherent noise (in ADC channels) assumed to be cell independent. The symbol $\mathcal{M}\{a\}$ denotes the mathematical expectation of value a and the symbols $\mathcal{C}\{a,b\} = \mathcal{M}\{(a - \mathcal{M}\{a\})(b - \mathcal{M}\{b\})\}$ and $\mathcal{D}\{a\} = \mathcal{C}\{a,a\}$ denote the covariance and dispersion. According to these definitions one has following trivial identities[8] $\mathcal{M}\left\{\mathcal{N}_i^{in}\right\} = 0$, $\mathcal{M}\left\{\mathcal{N}^{coh}\right\} = 0$, $\mathcal{M}\left\{\mathcal{S}_i^g\right\} = 1$, $\mathcal{C}\left\{\mathcal{N}_i^{in}, \mathcal{N}_j^{in}\right\} = 0$,

[6] The number of neighbour cells is 8 per 'regular' cells which are far from boundaries of Ecal regions, and it varies from 5 to 9 for cells near the boundaries

[7] Details on ECAL simulation, signal processing and digitization can be found elsewhere [2]

[8] The analogouse parametrisation is used in the digitisation procedure where "true" MC energy $\mathbf{e}_i$ is converted to "measured" energy ϵ_i

$\mathcal{C}\left\{\mathcal{N}_i^{in},\mathcal{N}^{coh}\right\}=0$, $\mathcal{C}\left\{\mathcal{S}_i^{g},\mathcal{N}^{coh}\right\}=0$, $\mathcal{C}\left\{\mathcal{S}_i^{g},\mathcal{N}_i^{in}\right\}=0$, $\mathcal{C}\left\{\mathcal{S}_i^{g},\mathbf{e}_j\right\}=0$, $\mathcal{C}\left\{\mathcal{N}_i^{in},\mathbf{e}_j\right\}=0$ and $\mathcal{C}\left\{\mathcal{N}^{coh},\mathbf{e}_j\right\}=0$, which are taken into account in equation (3).

Exploiting the parametrisation $\mathcal{D}\left\{\mathbf{e}_i\right\}=\mathbf{e}_i\times\mathcal{A}^2\times\mathrm{GeV}$, where $\mathcal{A}$ is a stochastic term in nominal calorimeter energy resolution, one can calculate the matrix elements $\mathcal{C}\left\{\epsilon_i,\epsilon_j\right\}$ using parameters $\mathcal{A}$, $\mathcal{G}_i$, $\mathcal{G}_j$, $\mathcal{D}\left\{\mathcal{S}_i^{g}\right\}$, $\mathcal{D}\left\{\mathcal{S}_j^{g}\right\}$, $\mathcal{D}\left\{\mathcal{N}_i^{in}\right\}$, $\mathcal{D}\left\{\mathcal{N}_j^{in}\right\}$ and $\mathcal{D}\left\{\mathcal{N}^{coh}\right\}$. From the matrix $\mathcal{C}\left\{\epsilon_i,\epsilon_j\right\}$ the 6 elements of symmetric 3×3 covariance matrix for values ϵ, x_b and y_b from equation (1) : $\mathcal{C}\left\{\epsilon,\epsilon\right\}$, $\mathcal{C}\left\{x_b,x_b\right\}$, $\mathcal{C}\left\{y_b,y_b\right\}$, $\mathcal{C}\left\{\epsilon,x_b\right\}$, $\mathcal{C}\left\{\epsilon,y_b\right\}$ and $\mathcal{C}\left\{x_b,y_b\right\}$ are determined analytically as functions of basic matrix $\mathcal{C}\left\{\epsilon_i,\epsilon_j\right\}$ elements. This 3×3 covariance matrix is the major basic ingredient for $\mathrm{e}^{\pm}$ identification [4].

The three elements of 2×2 symmetric matrix of the second order cluster momenta are evaluated in a similar way:

$$\mathcal{S}_{xx}=\frac{1}{\epsilon'}\sum_{\epsilon_i>0}x_ix_i\epsilon_i-x'_bx'_b\qquad\mathcal{S}_{xy}=\frac{1}{\epsilon'}\sum_{\epsilon_i>0}x_iy_i\epsilon_i-x'_by'_b\qquad\mathcal{S}_{yy}=\frac{1}{\epsilon'}\sum_{\epsilon_i>0}y_iy_i\epsilon_i-y'_by'_b,\quad(4)$$

where ϵ', x'_b and y'_b are evaluated according to[9]

$$\epsilon'=\sum_{\epsilon_i>0}\epsilon_i\qquad x'_b=\frac{1}{\epsilon'}\sum_{\epsilon_i>0}x_i\epsilon_i\qquad y'_b=\frac{1}{\epsilon'}\sum_{\epsilon_i>0}y_i\epsilon_i\qquad(5)$$

For degenerated clusters (only few cells with positive energy deposition or aligned placements of such cells along horizontal or vertical lines) $\mathcal{S}_{xx}$ and $\mathcal{S}_{yy}$ are set to be $\frac{S^2}{12}$, where S is the size of central cell in the cluster. This 2×2 matrix is used for selection of neutral clusters.

1.2 Neutral cluster selection

The selection of neutral clusters ("photon candidates") are performed using the matching techniques with reconstructed tracks.

All reconstructed tracks in the event are extrapolated to the calorimeter reference plane and then all-to-all matching with the reconstructed clusters are performed. The χ^2_{2D} is constructed[10]:

$$\chi^2_{\mathrm{2D}}\left(\vec{\mathbf{p}}\right)=\left(\vec{\mathbf{p}}_{tr}-\vec{\mathbf{p}}\right)^{\mathrm{T}}\mathcal{C}_{tr}^{-1}\left(\vec{\mathbf{p}}_{tr}-\vec{\mathbf{p}}\right)+\left(\vec{\mathbf{p}}_{cl}-\vec{\mathbf{p}}\right)^{\mathrm{T}}\mathcal{S}^{-1}\left(\vec{\mathbf{p}}_{cl}-\vec{\mathbf{p}}\right),$$

where $\vec{\mathbf{p}}_{tr}$ is the extrapolated track impact 2D-point to the calorimeter reference plane, $\mathcal{C}_{tr}$ is the covariance matrix of $\vec{\mathbf{p}}_{tr}$ parameters, $\vec{\mathbf{p}}_{cl}$ is cluster barycenter position (2D) and $\mathcal{S}$ is 2×2 cluster second momenta matrix, defined by equation (4) from section 1.1. The χ^2_{2D} is minimized with respect to $\vec{\mathbf{p}}$ and the value of χ^2_{2D} at minimum is used for selection of neutral clusters.

The clusters with minimal value of χ^2_{2D} estimator in excess of 4 are selected as neutral clusters ("photon candidates"). This cut rejects the clusters due to electrons and significantly suppress the clusters due to other charged particles keeping the high efficiency for clusters due to photons as shown on figures 1 and 2.

[9] Please note the difference between equations (1) and (5)

[10] This quantity is referred as χ^2_γ in references [4] and [5]

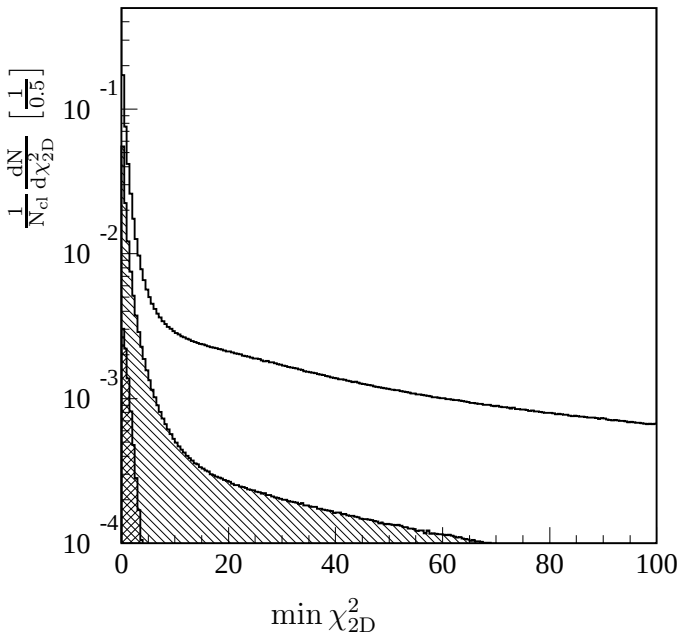

Figure 1: The minimal value of χ^2_{2D} estimator for all reconstructed clusters (open histogram) and the minimal value of χ^2_{2D} estimator for all reconstructed tracks (hatched histograms) and for reconstructed true MC electrons (cross hatched histogram).

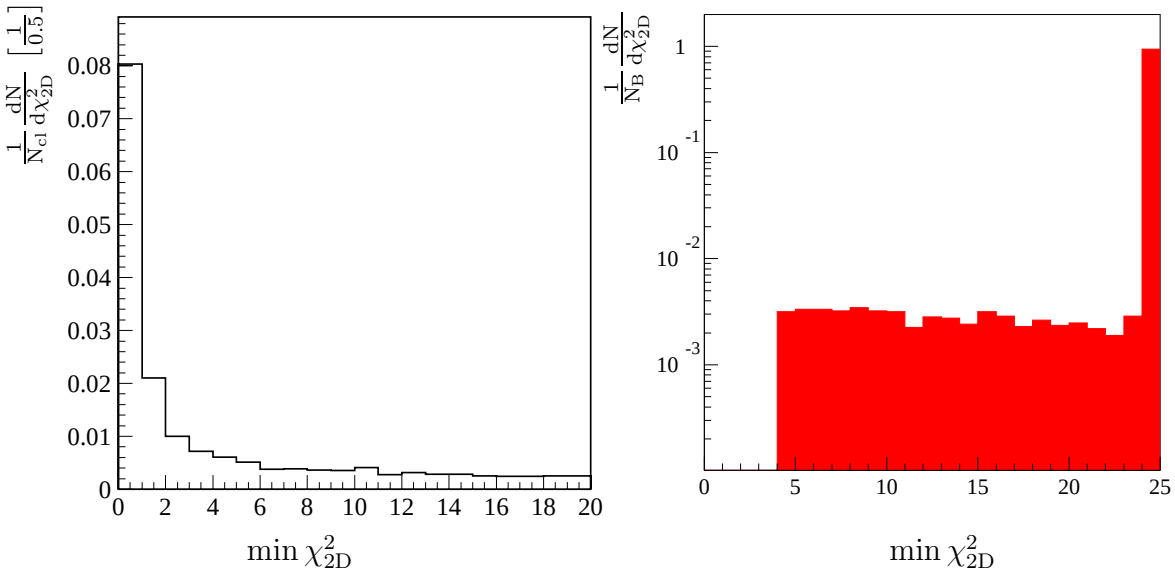

Figure 2: The minimal value of χ^2_{2D} estimator for reconstructed clusters associated with high-p_T photons from $B \to K^{*0}\gamma$ decay (left plot). The minimal value of χ^2_{2D} estimator for photons from reconstructed $B \to K^{*0}\gamma$ decays (right plot). Right bin includes all overflow entries.

1.3 Photon hypothesis reconstruction

Both energy and direction of photon are evaluated from the energy deposits in 3×3 cells around the cluster seed. Details are discussed below.

1.3.1 Photon energy

The photon energy, E_c, is evaluated from the total 3×3 cluster energy, $E_{3\times3}$, corrected from leakages according to the following relation :

$$E_c \;=\; \alpha\; E_{3\times3} \;+\; \beta\; E_{Prs}$$

where the parameters α and β accounts for energy leakages in Ecal and Preshower, respectively. Both parameters are evaluated in order that E_c matches on average the energy of isolated MC photons. The factor α is obtained from the photons subsample with no Prs hit (E_{Prs}=0). The passive-to-active energy factor β for Preshower is obtained from the complementary subsample once α is determined. It is found to be of the order of 8-9, depending on the Ecal region. The parameter α accounts for lateral and longitudinal leakages in Ecal and depends on the cluster energy ($E_{3\times3}$), the relative position of the energy-weighted barycenter inside the cluster ($\vec{r}_{b/seed}$) and inside the Ecal module frame ($\vec{r}_{b/module}$).
This threefold dependance is assumed to be separable as :

$$\alpha = \alpha_1(E_{3\times3}) * \alpha_2(\vec{r}_{b/cluster}) * \alpha_3(\vec{r}_{b/module})$$

where α_1 accounts for longitudinal leakages, while α_2 and α_3 account for the lateral shower extension outside the cluster area and the energy lost in the passive material between Ecal module, respectively.

As an illustration, the figure 3 displays the energy corrections, α_2 and α_3, as a function of the relative position of the energy-weighted barycenter. As can be seen, both the α_2 and α_3 corrections lie in the ± 5% range and are well fit with a linear function. As expected for α_2, smaller the cell size, larger the slope of the correction. In the X-direction, the α_3 slope is ±3% and ±2% on the boundary of the modules of the Inner (3×3 cell per module) and Middle (2×2 cells per module) Ecal regions, respectively. Due to the larger thickness of the module material in the Y-direction, larger slope of about ±5% and ±4%, are obtained, respectively. Such correction is no more needed in the Outer region where the module frame matches the cell granularity.
All the above corrections are evaluated depending on the Ecal region and take into account the eventual conversion of the photon. For that purpose the photons sample is split into two subsamples depending on the presence of SPD hit or not in the cell facing the Ecal cluster seed. The subsample without SPD hit mostly contains unconverted photons at 90%. In that case the energy resolution is found to be:

$$\sigma_E/E = \frac{(10.2 \pm 0.3)\%}{\sqrt{E}} \oplus (1.6 \pm 0.1)\%$$

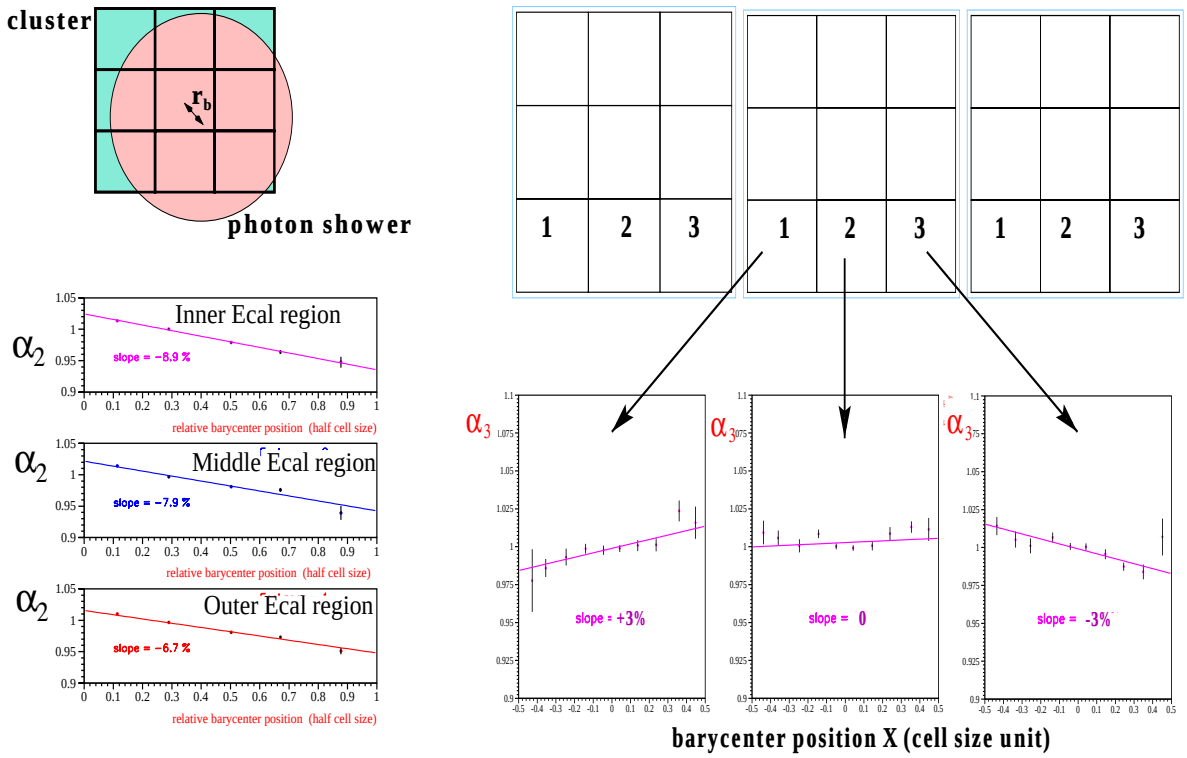

Figure 3: The energy corrections, α_2 and α_3 as a function of the relative position of the energy-weighted barycenter inside the cluster for the three Ecal regions (left) and inside the Ecal module frame for Inner Ecal region (right), respectively.

SPD hit indicates a late conversion at 79%. The corresponding resolution is then slightly degradated as shown on the left part of figure 8.

1.3.2 Photon momentum

The photon is assumed to come from the primary vertex and its direction is pointing to the 3D barycenter of the shower, (x_c, y_c, z_c), that is evaluated as explained below.

The longitudinal barycenter position, z_c, is obtained as the Ecal position corrected from the penetration depth of the photon (**L-correction**). The correction is scaled as the logarithm of the energy as :

$$z_c = z_{ecal} + \alpha \; ln(E_c) + \beta(E_{Prs}) \tag{6}$$

In order to take into account the information provided by the Preshower about the position of the shower begining, a smooth dependance of the parameter β with E_{prs} is included. Because of the large fluctuations of the longitudinal profile of showers, such a Preshower dependance leads to a limited gain on the position resolution.

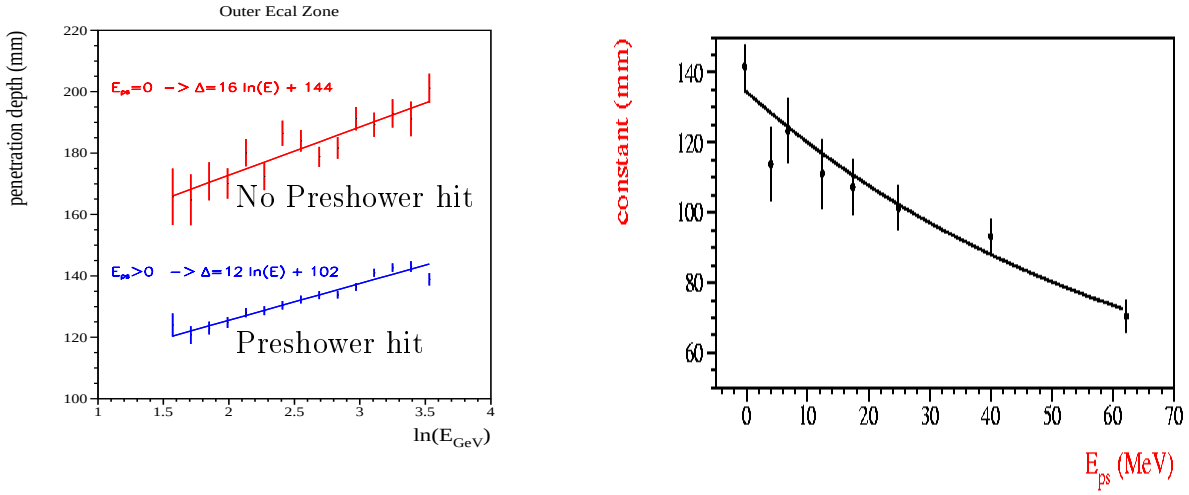

Figure 4: Longitudibal barycenter position as a function of the logarithm of the photon energy (left). Evolution of the parameter β as a function of the Preshower energy.

The average position of the shower barycenter inside the Ecal lies in the ∼10-20 cm range, depending on the photon energy and on the fact that the shower initiates within the Preshower or not. The left part of figure 4 displays the average barycenter position as a function of the logarithm of the photon energy. When Preshower is hit, the average penetration depth is 4 cm lower, in agreement with the Preshower thickness. On the right part of figure 4 the evolution of the parameter β with E_{prs} is shown.

The transversal barycenter of the shower, (x_c, y_c), is evaluated from the energy-weighted barycenter of the cluster corrected from the non linear transversal profile of the shower shape (**S-correction**). Assuming the transversal shower shape fit with a single exponential, $E(r) \sim E_0 e^{-r/\mathbf{b}}$, the S-corrected barycenter, (x_c, y_c), is then given by the single parameter $\mathcal{S}$-function [8] :

$$(x_c, y_c) = \mathcal{S}_0 \left[(x_b, y_b), \mathbf{b} \right] = \mathbf{b} \ \text{asinh} \left[\frac{(x_b, y_b)}{\Delta} \cosh \frac{\Delta}{\mathbf{b}} \right] \tag{7}$$

where (x_b, y_b) are the X/Y positions of the energy-weighted barycenter, Δ the half cell size and $\mathbf{b}$ the decay constant of the exponential profile. This $\mathcal{S}$-function is obtained by solving the system :

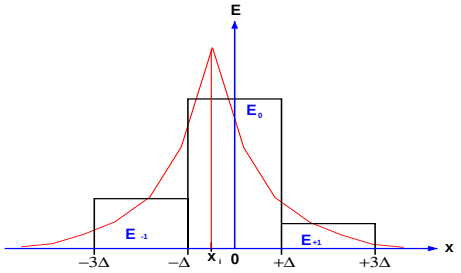

$$\left\{ \begin{array}{rcl} \varepsilon(x) & = & \varepsilon_0 e^{\frac{-\|x-x_i\|}{\mathbf{b}}} \\ x_b & = & \frac{2\Delta E_{+1} - 2\Delta E_{-1}}{E_{-1}+E_0+E_{+1}} \\ E_{-1} & = & \int_{-3\Delta}^{-\Delta} \varepsilon(x)dx \\ E_0 & = & \int_{-\Delta}^{\Delta} \varepsilon(x)dx \\ E_{+1} & = & \int_{\Delta}^{3\Delta} \varepsilon(x)dx \end{array} \right.$$

The **b** parameter is tuned in order that the reconstructed impact point on the Ecal front face, $(x_i, y_i) = (x_c, y_c) \times z_{ecal}/z_c$, matches the MC photon one, on average. It is found to be about 10%, 13% and 15% of the cell size for the Outer, Middle and Inner Ecal region, respectively.
Because the actual transversal shower shape is better fit with a double exponential function (see for example the figure 18 in the section 2.2), an additionnal corrections to S_0 is needed. In addition, the transversal barycenter position has to be corrected from left/right asymmetries in the X-direction (bottom/up in the Y-direction) that is due to the incidence angle of the photon that induce a non spherical profile of the shower spot.
Eventually the S-correction is given by :

$$(x_c, y_c) = \mathcal{S}_0[(x_b, y_b), \mathbf{b}] + \mathcal{S}_1[(x_b, y_b)] + \mathcal{S}_2[(x_b, y_b)] \tag{8}$$

where $\mathcal{S}_1$ and $\mathcal{S}_2$, iluustrated on the figure 5, correct from residual S-shape and geometrical assymetries, respectively.

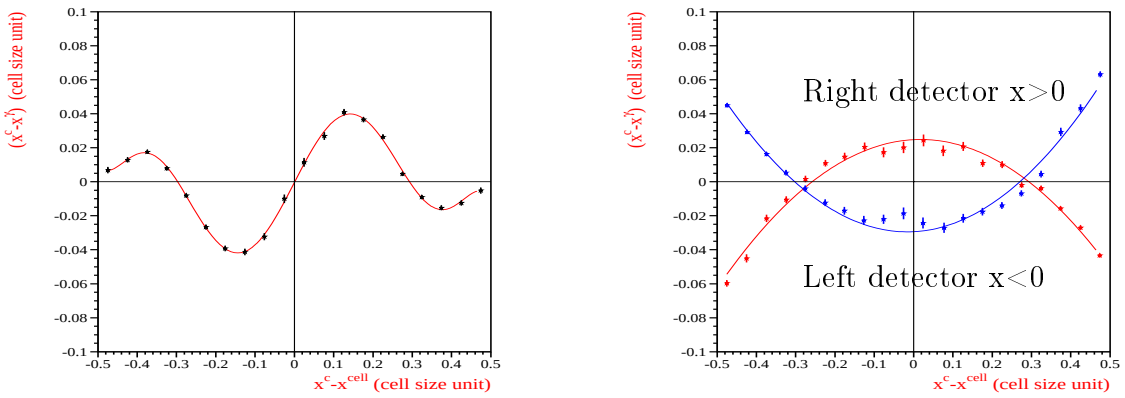

Figure 5: Example of the $\mathcal{S}_1$ (left) and $\mathcal{S}_2$ (right) corrections in the X-direction for the Outer Ecal region (see text for details).

Each $\mathcal{S}_1$ and $\mathcal{S}_2$ improve by 7% the resolution on the impact position of the photon from the $B_d \to K^*\gamma$ decay. For these photons spectrum an average resolution of 1.5mm,

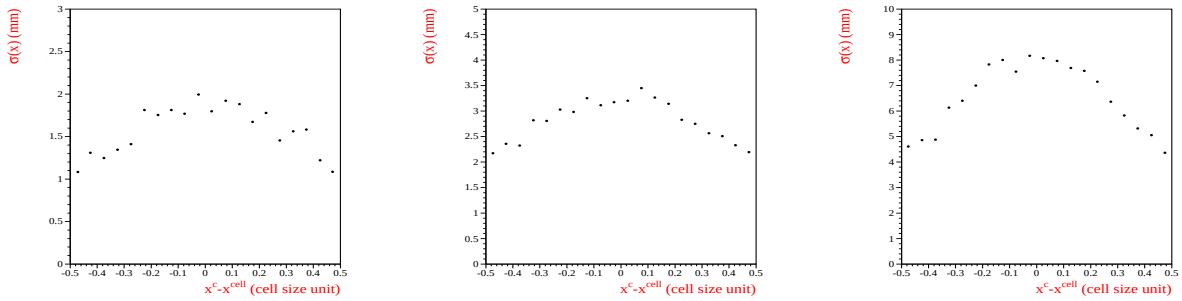

Figure 6: Transversal resolution versus the barycenter position for the photon coming from $B_d \to K^*\gamma$ decay for the three Ecal regions (inner, middle and outer from left to right respectively).

3mm and 7mm is obtained in the inner, middle and outer part of Ecal, respectively (i.e. $\sim$ 4%, 5% and 6% of the cell size). Figure 6 displays the resolution as a function of the barycenter position inside the cluster for the photons from the $B_d \to K^*\gamma$ decay.

The impact of the S-corrections and the L-corrections on the S-shape is displayed on figure 7.

The angular resolution as a function of the energy for non converted (no SPD hit) and converted (SPD hit) photons is displayed on the right part of figure 8.

The photon 4-momentum is evaluated from (E_c, x_c, y_c, z_c) assuming the photon is coming from the interation point. All the above described energy corrections, S-corrections and L-corrections are propagated to the covariance matrices computation .

1.4 Photon identification

Photons in the detector are first identified according to their isolation with respect to charged particles. A 2-dimensional $\chi^2_{\rm 2D}$ based on the geometrical distance between the cluster position and the extrapolation of the reconstructed tracks up to the calorimeter is built. Photon candidates are required to verify $\chi^2_{\rm 2D} > 4$. The background (mainly hadrons) is large and this cut removes a large part of it. The remaining photon background has a low P_t.

Two types of photons can be distinguished : converted and not converted ones.

1.4.1 Conversions

The matter before the calorimeter is the source of photon conversions. Two types of photon conversions clearly appear :

- Conversion before the magnet :
  The pair of electrons are swept away by the magnetic field or are seen as two charged

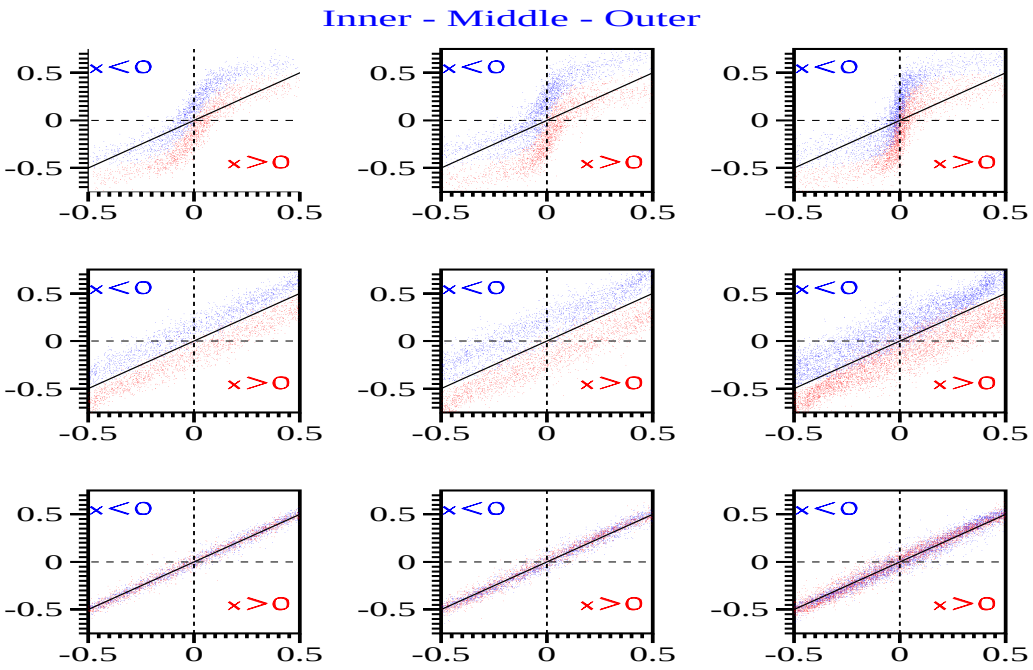

Figure 7: The barycenter versus MC impact position (cell size unit) in the X direction (top figures). Same after S-corrections (middle figures) and L-corrections (bottom figure). From left to right : inner, middle and outer Ecal region. Photons in the left (x<0) and the right (x>0) part of the Ecal are indicated.

clusters in the calorimeters. The LHCb tracking system may reconstruct the corresponding electron tracks.

- Conversion after the Magnet :
  The electron impulsions are not so strongly affected by the magnetic field. According to the position along the Z-axis of the photon decay a single cluster may be seen. Usually no track is reconstructed.

In the following, we define Monte Carlo converted γ, the photons that decayed before the PRS lead absorber ($Z = 12380$ mm). Two techniques can be used to identify the converted photons :

- Reconstructed tracks of the produced electrons.
- SPD information on the charge of the incoming particle.

Up to now, the second technique only is used in the analysis. The electrons converted before the magnet may produce reconstructible electron tracks. However, the χ^2_{2D} cut on the clusters cut away those converted photon candidates. In the future, a dedicated algorithm should aim at identifying those electron pairs. Electrons produced after the

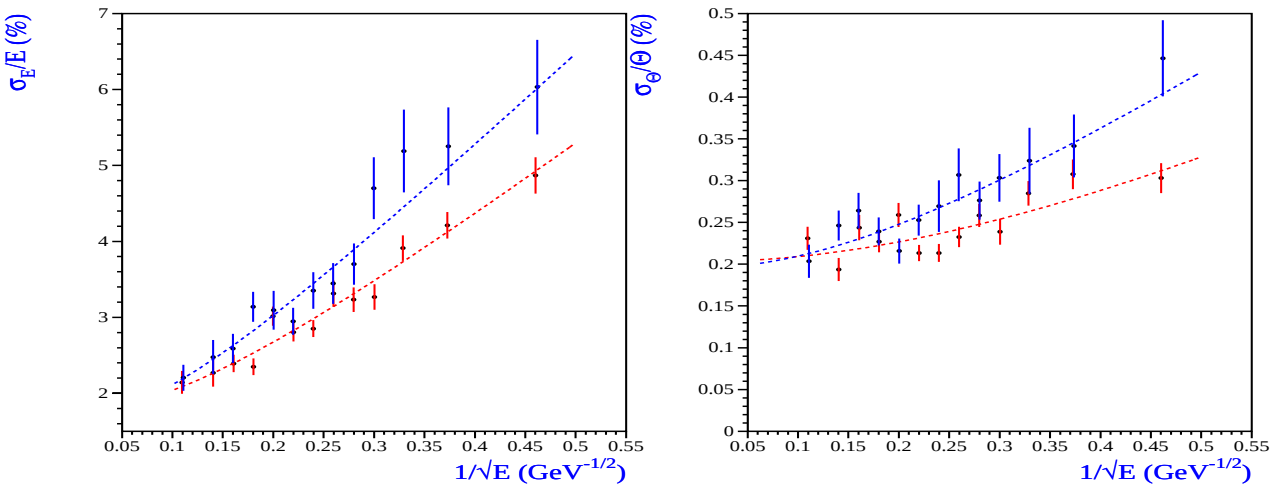

Figure 8: The energy (left) and angular (right) resolution as a function of the energy for the photon from $B_d \to K^*\gamma$ decay. The red points corresponds to the photon clusters with no SPD hit in front of cluster seed (unconverted photons at 90%) and blue points corresponds to the SPD hit case (converted photons at 79%).

magnet and *a fortiori* after the tracking chambers are usually not reconstructed. The two electrons of the pair will usually make a single cluster in the electromagnetic calorimeter (see figure 9).

The SPD provides the information on the charge of the incoming particle and allows to identify that a conversion took place. It is then possible to apply different calibration to electrons and photons and thus to converted and not converted candidates. As can be seen on figure 10, on average 44% of the photons originating from the interaction point are converted when reaching the lead absorber of the PRS. In terms of radiation length, this corresponds to $70\%X_0$. Among the converted γ, half of them decay before the magnet. The proportion of converted photons seems to increase with respect to the P_t^γ. This could be partially explained by the geometric increase of thickness crossed by higher angle particles. This could also be due to the fact that the amount of material in the detector is not uniform with respect to η (i.e. the M1 muon chamber granularity is higher in the central region than in the outer leading to a large increase of matter at large η).

As was already pointed out, the distinction between not converted and converted γ is only based on the SPD information in the cell facing the seed of the cluster of the reconstructed photon. The electron or photon shower calibration are also performed with respect to the SPD signal. The 10% pollution level in the not-converted case could be understood by the SPD occupancy or by the backsplash effect. The fact that 20% of the converted are not correctly identified is more difficult to explain. However, it was noticed that the impacts of the two electrons is sometimes not in the seed cell but rather on the neighboring (right or left according to the particle charge and detector magnetic field

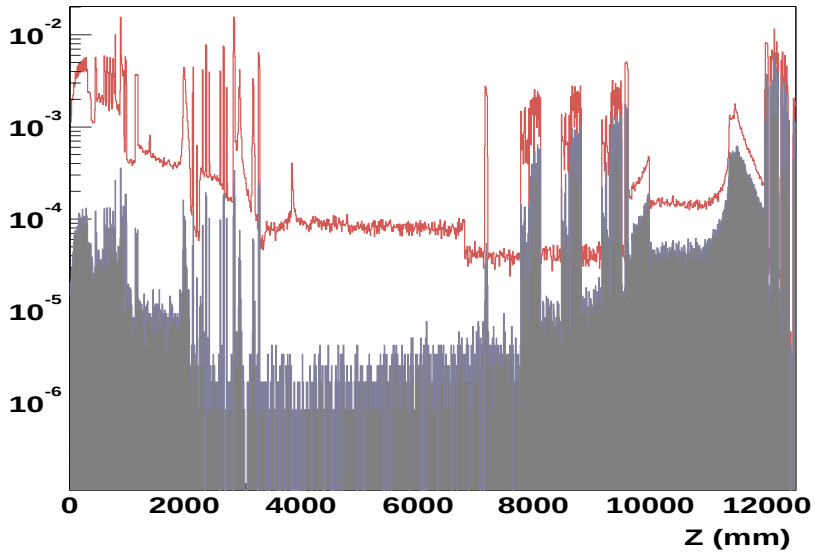

Figure 9: The red histogram shows the repartition of the photon conversions along the Z-axis. A bin corresponds to 1cm and the main structures of the detector can be clearly identified. The blue histogram shows, among the previous converted photons, those that can be associated to a single cluster in the calorimeter and whose energy equals the Monte Carlo photon energy ±25%.

direction) ones.

In a $B_d \rightarrow \pi^+\pi^-\pi^0$ event, 3 correctly identified photons out of 4 are not converted ones. We recall that photons converted before the magnet are never reconstructed. Thus, as shown on plot 11, the absolute contamination of the not converted reconstructed photons is lower than in the converted case.

1.4.2 Photon Identification

As already explained, photon identification is done in a first stage by an anti-coïncidence between the cluster position and the extrapolation of the reconstructed tracks up to the calorimeter. The only tools remaining to select photons rely on the combination of the SPD, PRS and shower shape information. Shower shape is intensively used to identify the merged π^0. Figure 12 shows the effect on the signal (both converted and not converted) and the background of various cuts based on the SPD/PRS signal. The left (first) column is the number of photons reconstructed after the tracking veto.

The photon reconstruction efficiency and purity are shown for three cuts (tracking veto, veto and two PRS energy cuts at 4 and 10 MeV) on figure 13 for the not converted case and thr converted one. Purity is only slightly different between converted and not converted photons, as can be seen from the right plots. The main difference appears when looking at reconstruction efficiencies on the left plots, as most of the photons converted before

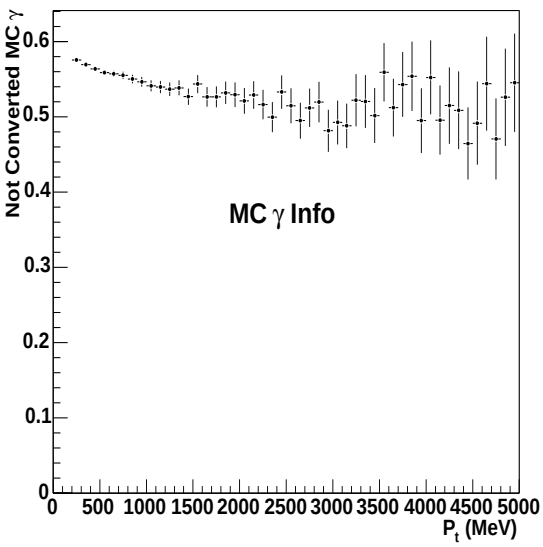

Figure 10: Proportion of photons that do not convert before the calorimeter among the photons originating from the interaction point (50000 $B_d \to \pi^+\pi^-\pi^0$ events) versus P_t^γ.

Table 1: The photons reconstructed are correctly identified as (not) converted in (90%) 80% of the case by the SPD signal in the cell facing the seed -central cell- of the 3×3 cluster of the reconstructed photon.

Associated MC γ	Statistics	no SPD hit	SPD hit
$\gamma \nrightarrow ee$	454445	90.0%	10.0%
$\gamma \to ee$	152617	20.9%	79.1%

the magnet produce electrons that are swept out from the acceptance of the calorimeter by the magnetic field. As roughly half of the conversions take place before the magnet the converted photon efficiency is divided by a factor 2. After the magnet, the converted photons are identified with the same probability as the not converted ones.

The energy correction applied on the photon candidates depends on the converted or not converted gamma hypothesis. The candidates are sorted out according to the measurement in the SPD cell facing the cluster seed of the photon, i.e., the local maxima which is also the central cell of the 3×3 zone.

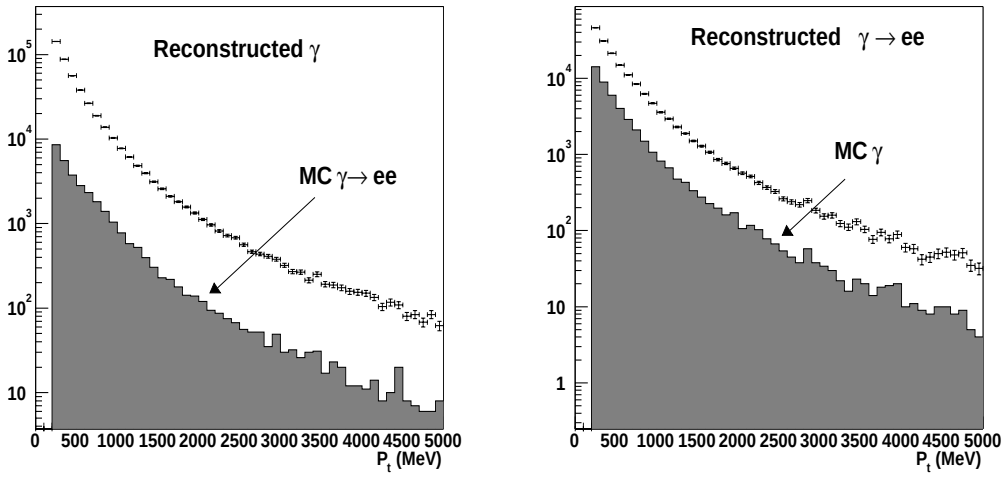

Figure 11: P_t dependence of the not-converted/converted identification by the SPD signal. There is almost no variation in the reconstructed γ case.

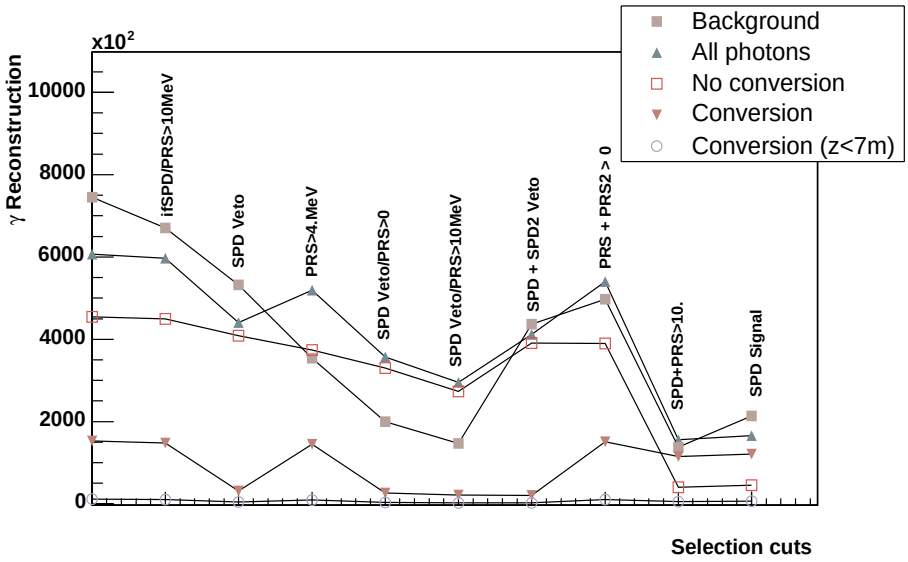

Figure 12: Effect of various cuts on some combinations of the SPD/PRS signals. The left column corresponds to the number of reconstructed photons after the tracking veto. The name *SPD2* means constraining (by a veto or requesting a hit) the signal of a second cell in SPD in front the ECAL cluster ; *PRS2* is the energy measured in the second highest energy cell in the PRS in front of the ECAL cluster.

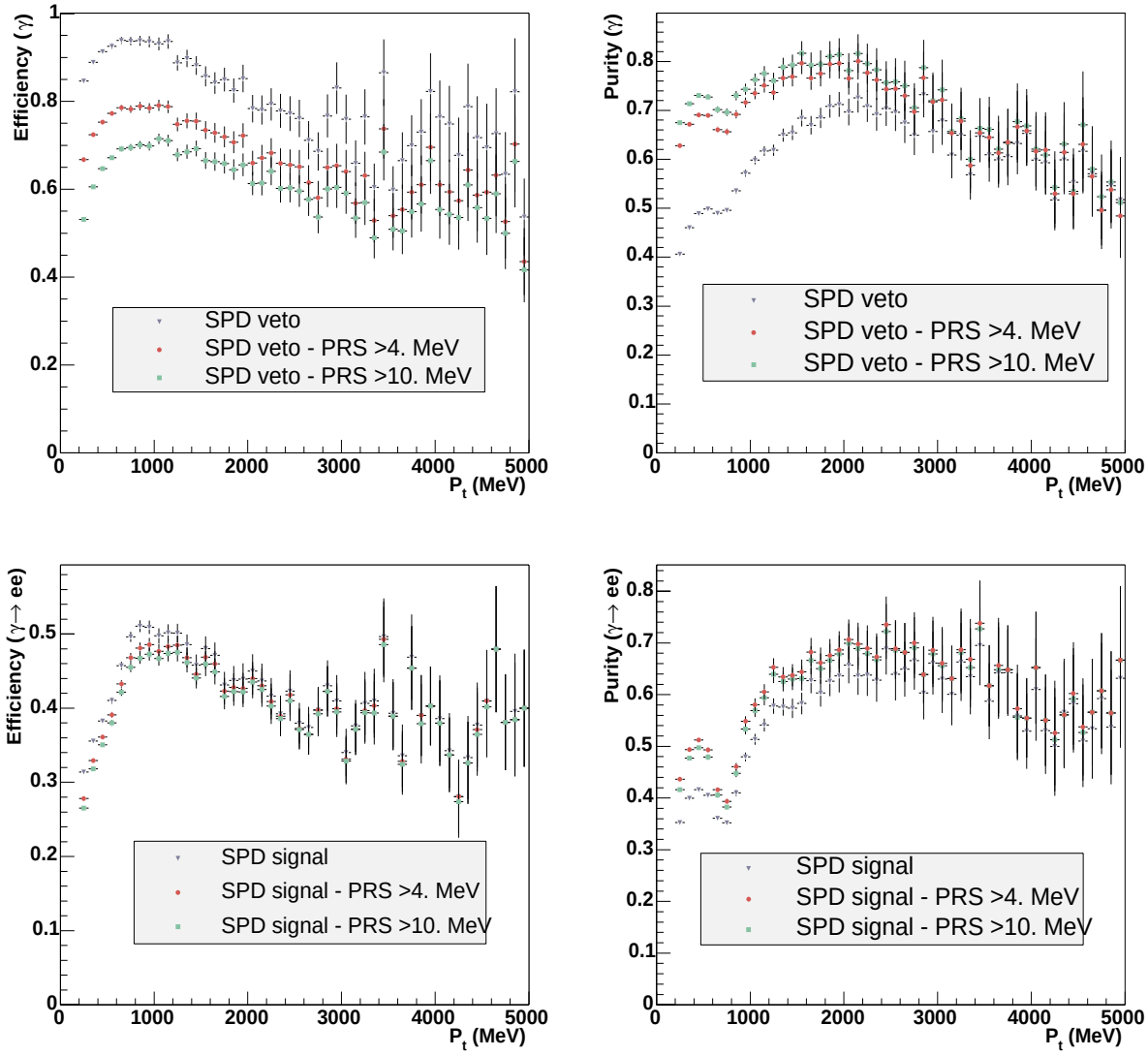

Figure 13: Photon reconstruction efficiency (left) and purity (right) for not converted photons (top) and converted ones (bottom). The three curves correspond to three different cuts applied : tracking veto alone, veto and two PRS cuts at 4 and 10 MeV.

2 Neutral pions reconstruction

The mean transverse momentum of the neutral pion from the $B_d \to \pi^+\pi^-\pi^0$ decay is about 3 GeV. Below this value the π^0s are mostly reconstructed as a resolved pair of well separated photons. On the opposite, a large fraction of the pairs of photons coming from the decay of high energy π^0s cannot be resolved as a pair of clusters within ECAL granularity. About 30% of the reconstructible π^0 from $B_d \to \pi^+\pi^-\pi^0$ signal lead to a single cluster. Such a configuration, hereafter referred as "merged", essentially appears for π^0 above 2 GeV/c in P_t.
Figure 14 displays the transverse momentum of the reconstructible π^0 from the $B_d \to \pi^+\pi^-\pi^0$ decay. The respective contributions of resolved and merged configuration is indicated.

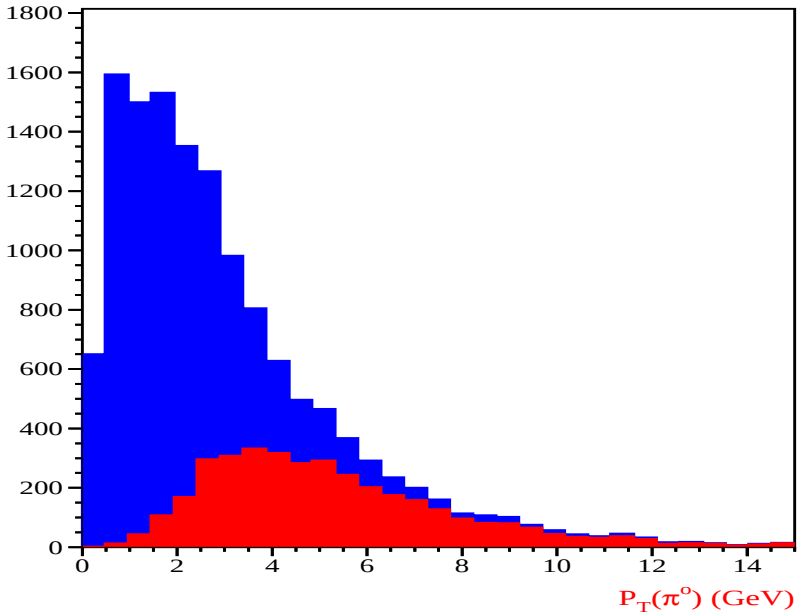

Figure 14: Transverse momentum of the reconstructible neutral pion from the $B_d \to \pi^+\pi^-\pi^0$ decay. The contribution of resolved and merged π^0 is indicated with blue and red histograms, respectively.

The reconstruction and identification of resolved and merged π^0 are discussed in the two following subsections, respectively.

2.1 Resolved π^0

The lowest energy π^0 produced at the LHCb interaction point are reconstructed in the Calorimeter as two separated clusters corresponding to the two photons of the neutral π desintegration. The procedure used to make the π^0 is first to reconstruct photon candidates, then loop over the candidates, pair them and compare the corresponding invariant masses with the nominal π^0 mass. Among the photon candidates, only those whose P_t is greater than 200 MeV/c are kept and paired to reconstruct π^0. Except from the tracking veto described in the previous sections, no other cut is applied to select γ with a better purity at the cost of a lower efficiency. In the $B_d \to \pi^+\pi^-\pi^0$, the wrong π^0 reconstruction is due essentially to combinatorial background of real photons or fragmentation π^0 and not to pairing of background clusters.

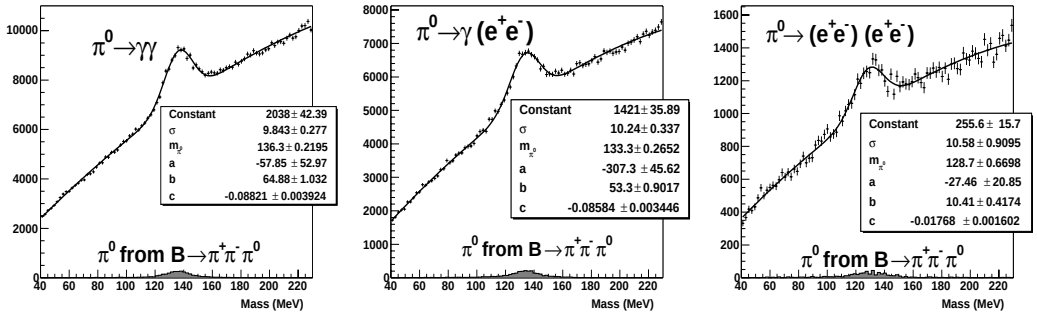

Figure 15: π^0 Mass distributions in the three distinct reconstruction cases (from left to right plot) : no conversion, one γ converted and both γ converted before the calorimeter. The separation converted/not converted is obtained from the SPD information. The curves are fitted with a Gaussian and a third degree polynom. The contribution of true π^0 originating from the $B \to \pi^+\pi^-\pi^0$ decay are showed at the bottom of the distributions.

Figure 15 shows the mass distributions obtained in the three cases where both photon candidates reached the calorimeter (left), one converted (center) or both converted before the calorimeter (right) according to the SPD signal. The contributions of true π^0 is roughly 20% of the distribution in the range $m_{\pi^0} \in [105, 165]\,\mathrm{MeV}/c^2$, the remaining contribution being due to background cluster pairings and γ combinatorial background. The curves have been fitted by the sum of a Gaussian and a polynomial function and lead to a sigma for the π^0 mass of 10 MeV/c^2. The plots also show the contributions of true π^0 originating from B mesons decaying in the $B_d \to \pi^+\pi^-\pi^0$.

The resolved π^0 identification efficiency (showed together with the purity on figure 16 and applying three photon cuts: the default tracking veto cut, and adding two types of PRS energy cuts. On this figure, the normalization is on the total number of π^0, resolved and merged) depends strongly on P_t. At low P_t, one of the two γ is more likely to be smaller than the P_t cut of 200 MeV/c^2 applied on photon candidates. Such a cut is nevertheless necessary in order to reduce combinatorial background. At high P_t, the photons produced

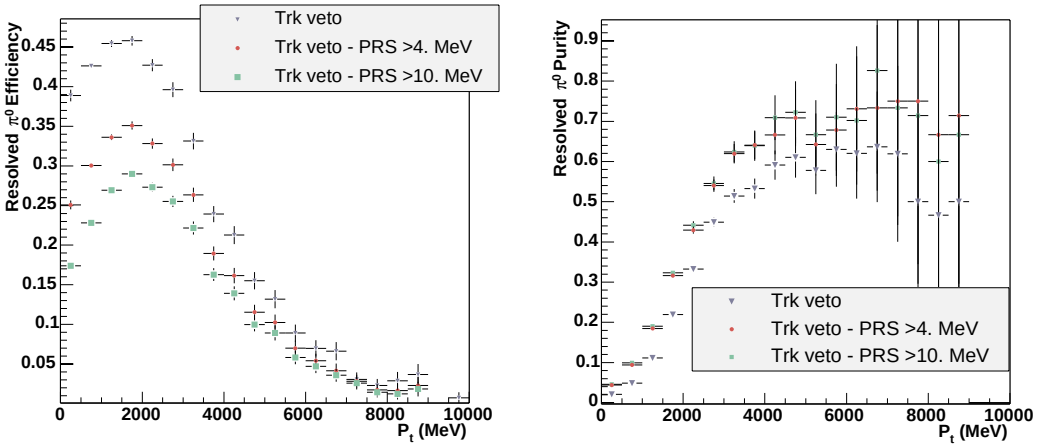

Figure 16: The π^0 efficiency (here defined as the number of resolved π^0 identified in the ± 30 MeV/c^2 mass window over the total number of π^0, resolved and merged in the detector acceptance) and the purity versus the π^0 transverse momentum. At P_t greater than 2 GeV/c more and more π^0 are reconstructed as merged π^0 and are not counted in this plot. Three photon cuts are applied : the default tracking veto and adding two types of PRS energy cut in the PRS cell facing the seed of the cluster.

by π^0 decays are more likely to be merged and are not identified by the pairing method.

The contributions of the three π^0 types (none, one and two conversions) among the resolved π^0 selected and produced in the $B \to \pi^+\pi^-\pi^0$ decay is shown on figure 17. The obtained π^0 mass width is of the order of 9 MeV/c^2 performing a two gaussian fit of the distribution.

2.2 Merged π^0

2.2.1 Merged π^0 reconstruction

An efficient reconstruction of merged π^0 is of major importance for $B_d \to \pi^+\pi^-\pi^0$ selection, on account of their intrinsic large transverse energy [9].
For that purpose, a procedure has been designed to disentangle a potential pair of photons merged into the single clusters.

The algorithm consists in spliting each of the Cellular Automaton single clusters into two interleaved 3×3 subclusters built around the two main cells of the original cluster (see figure 18). The energy of the common cells is then shared among the two virtual subclusters according to an iterative procedure based on the expected transversal shape of photon showers. The sharing of the energy depends on the barycenter position of each subcluster that is a function of the energy sharing. The procedure is looping over few iterations and is fastly converging.
The expected transversal shower shape is obtained from a sample of isolated photons as

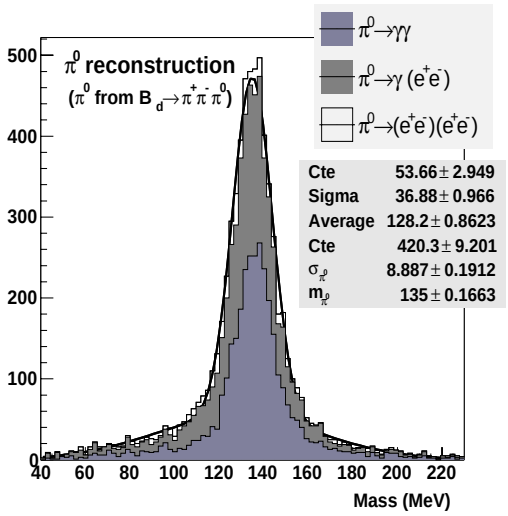

Figure 17: Resolved π^0 mass distribution obtained from pions selected by the default tracking veto and produced by $B_d \to \pi^+\pi^-\pi^0$ decay. As shown, the fitted (double gaussian fit) sigma is of the order of 9 MeV/c^2.

the fit of the energy deposit as a function of the distance to the cluster barycenter. The transversal shower profiles used as input for the merged π^0 reconstruction algorithm is shown on the figure 18 for the three Ecal region, respectively.

Each of the two subclusters is then reconstructed as a single photon hypothesis cluster In particular, the energy corrections , L-corrections and S-corrections detailed in section 1.3 are applied to the merged photons reconstruction. This method has been shown to improve over other analytical method based on the moment analysis of the cluster shape which requires shower symmetries (see appendix A).

The left part of figure 19 displays the invariant mass obtained from all single clusters in $B_d \to \pi^+\pi^-\pi^0$ events. The clear bump around 135 MeV/c^2 contains the contribution from the merged pairs of photons from π^0 decays. The right part shows the same distribution for the cluster associated to the MC π^0 from the B_d decay. The distribution is well fit by two Gaussian functions, to account for the broadening of the resolution due to photon(s) conversion. The shaded histogram indicates the contribution from pairs of photons with at least one conversion. A core resolution of about 15 MeV/c^2 is obtained.
The reconstruction of the 4-momentum of merged π^0 is competitive with resolved configuration. The energy resolution is consistent with the single photon resolution, as expected. The direction resolution is smaller than 1 mrad for merged π^0 above 20 GeV.

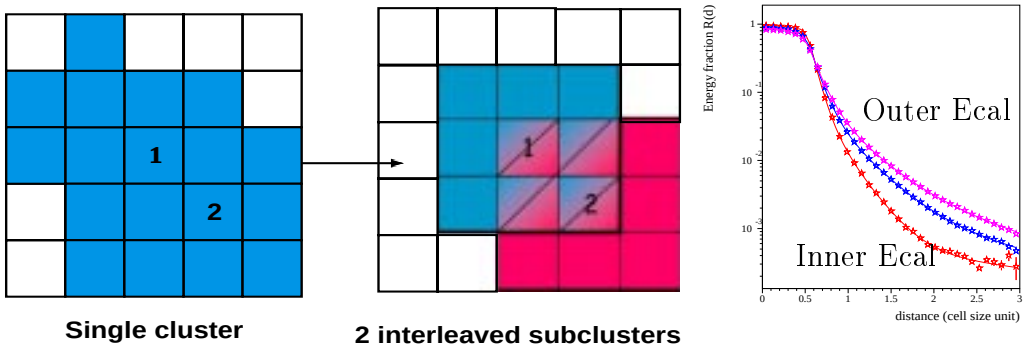

Figure 18: The subclusters building from single cluster. The two main cells whith the higher energy deposit are identified and two interleaved 3×3 subclusters are built around each of them. The energy sharing of the common cells of the two interleaved subclusters is done according to an interative procedure based on the transversal shower profile obtained from a sample of isolated photons for the three Ecal region, respectively (right figure).

2.2.2 Merged π^0 identification

As seen on the left histogram of figure 19, the merged π^0 have to be identified within a large 'combinatorial' continuum. This is achieved by applying criteria based on the π^0 energy, the neutral origin of cluster and a mass window. The identification of merged π^0 benefits from several features with respect to resolved case. First of all is the large transverse energy required by the π^0 to be merged. Second is the much lower combinatorial background : $\sim$60 clusters per events to be compared to $\sim$2000 pairs. Eventually, the identification criteria such as cluster neutrality is applied to a single cluster while a pair of clusters is involved for resolved π^0 and the corresponding efficiency is then squared. As a consequence of the intrinsic purity of the merged π^0, a quite large efficiency can be preserved for identification. For that purpose, the following criteria are applied :

- The cluster has to be neutral by requiring that its position is not consitent with a charged track. The $\chi^2_{\rm 2D}$ of the cluster-track matching (see section 1.2) is required to be greater than unity.
  The distribution of the corresponding confidence level is shown on figure 20 for $B_d \rightarrow \pi^+\pi^-\pi^0$ events.

- The π^0 energy is required to be compatible with a pair of merged photons. For that purpose, a cut is applied on the minimal distance between the impacts of the two photons on the Ecal front face that is kinematically allowed for a π^0 decay :

$$d_{\gamma\gamma} = 2 \times z_{Ecal} \times m_{\pi^0}/E_{\pi^0} < 1.8 \;\; cell \;\; size.$$

  where z_{Ecal} is the longitudinal position along the beam axis of the Ecal front face (z_{Ecal}=12520 mm) This cut is fully equivalent to an energy cut of 45 GeV , 30 GeV

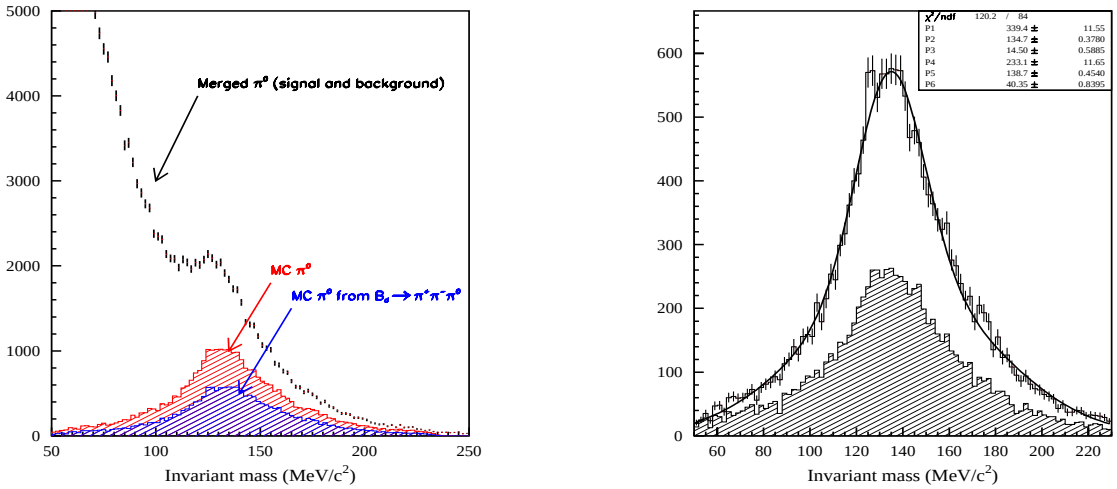

Figure 19: Left : invariant mass obtained with the merged π^0 algorithm for all clusters in $B_d \to \pi^+\pi^-\pi^0$ events. Right : same distribution for clusters associated to the π^0. The shaded histogram indicates the contribution from pairs of photons with at least one conversion.

and 15 GeV in the inner, middle and outer Ecal region, respectively. It is also roughly equivalent to a 2 GeV/c P_t cut. The $d_{\gamma\gamma}$ cut is however more efficient against combinatorial background than a P_t cut while the P_t cut is more efficient to separate the π^0 from the B decay from the other π^0.
The distribution of $d_{\gamma\gamma}$ is shown on figure 20 for $B_d \to \pi^+\pi^-\pi^0$ events.

- The invariant mass of merged photons is required to be compatible with the π^0 mass. Due to the fact that the combinatorial continuum sharply decreases at high mass, an asymmetrical window around the nominal π^0 mass improves the rejection of background. The merged π^0 mass is then required to be reconstructed in the $95 - 215$ MeV/c^2 mass range.
The distribution of the invariant mass is shown on figure 20 for $B_d \to \pi^+\pi^-\pi^0$ events.

The multiplicity of π^0 reconstructed and identified as merged is low and does not exceed the few candidates per event. The above criteria however preserves a quite large efficiency and purity. Almost 70% of the merged π^0 are reconstructed and identified ($\sim 80\%$ when both photons are not converted). The left part of the figure 21 displays the $\gamma - \gamma$ distance on the Ecal front face for the reconstructible π^0s. The fraction that are reconstructed and identified as resolved and merged are indicated by the blue and red contribution, respectively.

The overall efficiency to reconstruct and identify a π^0 that decay in the Ecal acceptance with both photons having P_t greater than 200 MeV/c is shown on the right part of the figure 21 as a function of $P_t(\pi^0)$. The separate contribution from resolved (see also

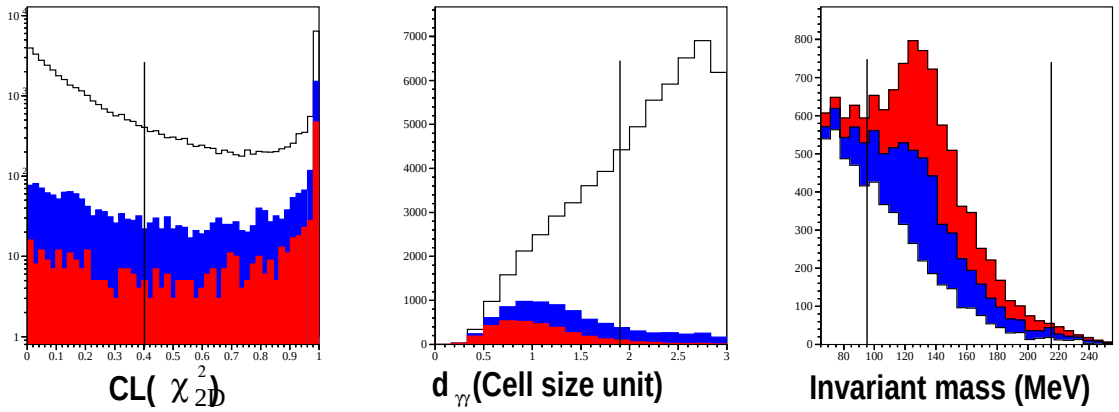

Figure 20: Distribution for $B_d \to \pi^+\pi^-\pi^0$ events of the three variables used for merged π^0 identification : the cluster-track matching confidence level : CL(χ^2) (left), the minimal $\gamma - \gamma$ distance : $d_{\gamma\gamma}$ (middle) and the invariant mass (right). On each plot the vertical lines indicate the cut applied for the merged π^0 identification. The separate contribution from the π^0 coming from the B_d decay, the other π^0s and the combinatorial background, are indicated by the the red, blue and white part, respectively.

figure 16) and merged π^0 reconstruction are indicated by the solid and dashed histograms, respectively. The average efficiency for the π^0 coming from the $B_d \to \pi^+\pi^-\pi^0$ decay is 52.8% (32.8% from resolved + 20.0 % from merged π^0).

The left histogram of figure 22 displays the reconstructed mass for π^0 identified candidates in $B_d \to \pi^+\pi^-\pi^0$ events. The breakdown of the various contributions are indicated. As can be seen, the overall π^0 purity is 63% for the $B_d \to \pi^+\pi^-\pi^0$ events. About half of this are π^0 from the $B_d \to \pi^+\pi^-\pi^0$ signal. The combinatorial background is essentially coming from single photons, possibly overlapping with other particles. The purity is shown as a function of the P_t on the left part of figure 22.

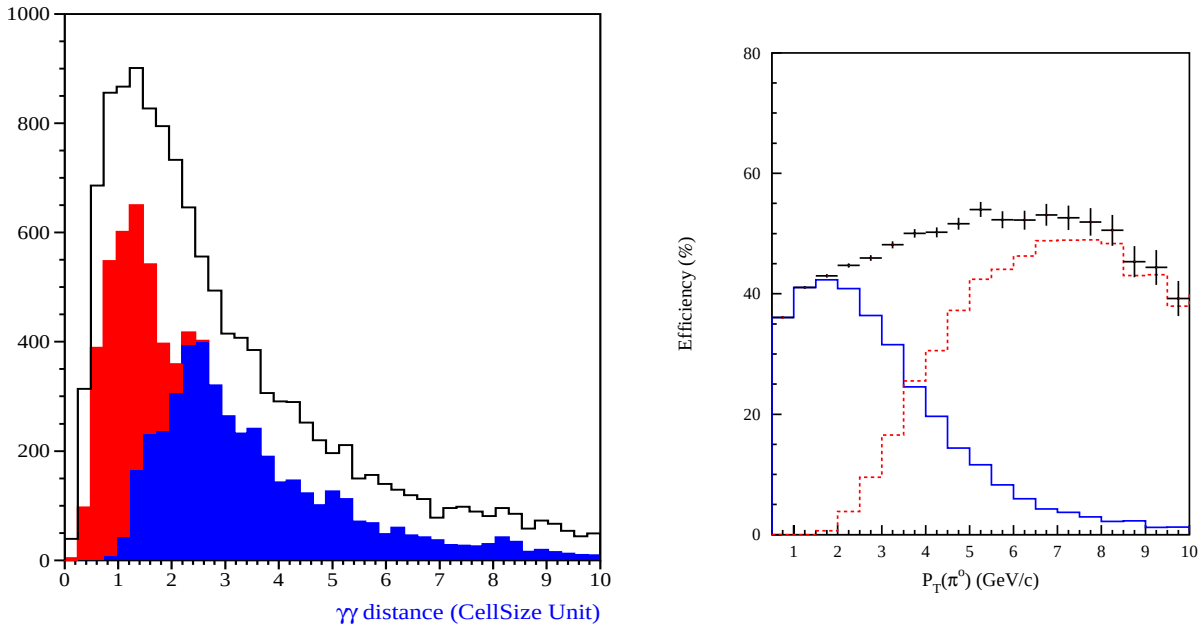

Figure 21: Left : the $\gamma - \gamma$ distance (cell size unit) on the Ecal front face for the reconstructible π^0s. The fraction that are reconstructed and identified as resolved and merged are indicated by the blue and red contribution, respectively. Right : overall π^0 efficiency (defined as the number of π^0 identified in the mass window over the number of π^0 in the detector acceptance with $P_t(\gamma) > 200$ MeV/c). The separate contributions from resolved and merged π^0 reconstruction are indicated by the solid and dashed histograms, respectively.

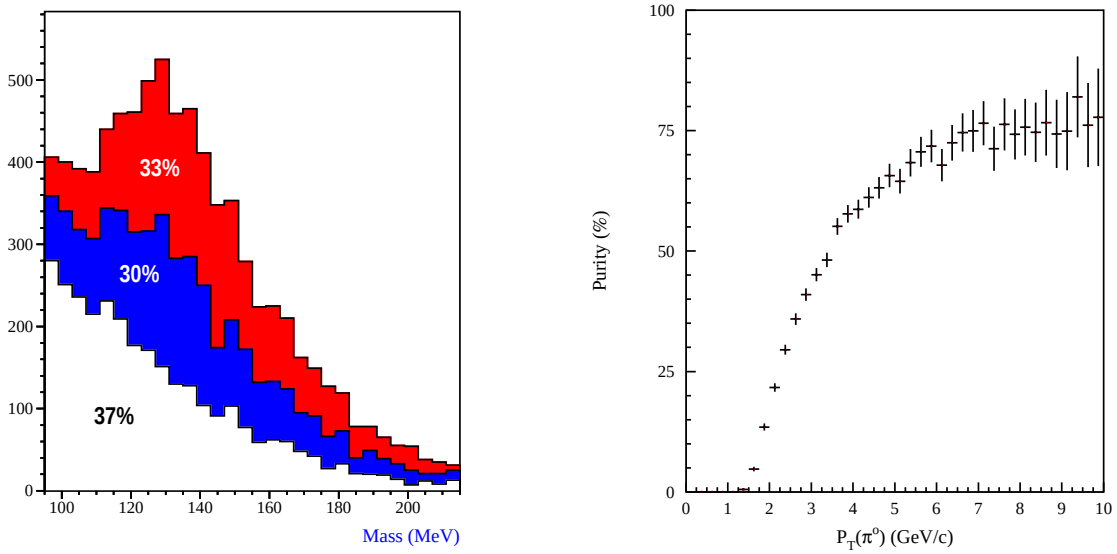

Figure 22: Right : mass distribution for the π^0 candidates reconstructed and identified as merged in $B_d \to \pi^+\pi^-\pi^0$ events. The red part of histograms represents the contribution due to the π^0s from $B_d \to \pi^+\pi^-\pi^0$ signal and accounts for 33% of all the identified merged π^0 candidates. The blue part, 30% represents the other π^0s and the combinatorial background accounts for the remaining 37% (white part). Left : the merged π^0 purity as a function of the P_t.

2.3 Robustness studies

No separate calorimeter specific robustness studies were performed. For the Global Robustness Test, described in detail in [5] the level of coherent and incoherent noise was varied for calorimeter channels, and conservative estimates of the percentage of dead channels were used. In addition the unknown detector and calibration imperfections were combined into an effective parameter, referred to as "gain error" which appears as an additional constant term into the energy resolution of the channel.

The nominal values of these parameters and their setting for Global Robustness Test are listed in Table 2.

Table 2: Calorimeter specific parameters of Global Robustness Test

Calorimeter	Nominal	Robustness
Incoherent noise r.m.s. [ADC counts]		
PRS	1.0	1.5
ECAL	1.2	1.5
HCAL	1.2	1.5
Coherent noise r.m.s. [ADC counts]		
PRS	0	0.5
ECAL	0.3	0.5
HCAL	0.3	0.5
Dead channels [%]		
SPD	0	1.0
PRS	0	1.0
ECAL	0	0.2
HCAL	0	0.2
'Gain error' [%]		
SPD	0	1.5
PRS	1	1.5
ECAL	1	1.5
HCAL	1	1.5

2.4 Robustness test for photons

In robustness analysis the reconstruction algorithm and selection requirements [6] for $B \to K^{*0}\gamma$ were not changed, however trigger thresholds were re-tuned to satisfy the constraints: 1 MHz output rate after L0 and 40 kHZ output rate after L1 [7].

Loss in overall selection efficiency was obtained to be 5%, while the total efficiency loss with L0 and L1 trigger applied was 28%. Degradation in B^0 mass resolution was found to be 7% both with and without triggers applied (Figure 23).

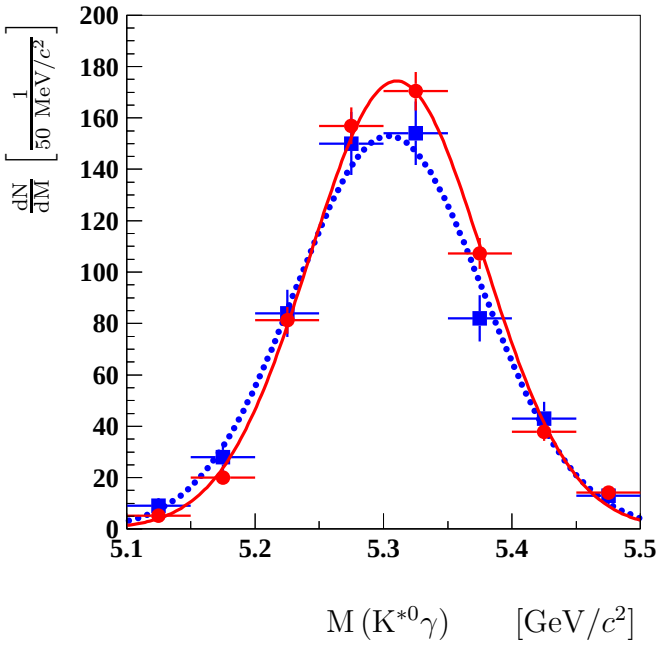

Figure 23: $K^{*0}\gamma$ mass distribution after off-line cuts (without trigger) for $B \rightarrow K^{*0}\gamma$: default detector performance with B^0 mass resolution 68 MeV/c^2 (red points and solid line); "global robustness" test with B^0 mass resolution 73 MeV/c^2 (blue boxes and dashed line). Both distributions are normalized on 50K signal events before reconstruction.

2.5 Robustness test for neutral pions

The performance of π^0 reconstruction and identification has been tested on a specific "robustness test" sample of 50k $B_d \rightarrow \pi^+\pi^-\pi^0$ events.

Figure 24 displays a comparison of the reconstructed π^0 mass between the generic and the specific samples. For both resolved and merged π^0, the "robustness" resolution is slightly degradated with respect to the "default detector" sample and the peak position is slightly miscalibrated (as the photons corrections are not retuned for robustness test configuration). The reconstructed mass distribution is fit with two gaussians which parameters are detailed in table 3. Degradation of the core resolution is found to be $\sim$ 14% and $\sim$19% for resolved and merged π^0s, respectively. Note that this degradation is of the same magnitude level than the statistical uncertainty due to the limited size of the "robustness test" sample.

With the "robustness test" sample, the overall efficiency to reconstruct and identify a π^0 from the $B_d \rightarrow \pi^+\pi^-\pi^0$ signal that decay in the Ecal acceptance with both photons having P_t greater than 200 MeV/c is found to be 52.3% (19.3% from merged + 33.0% from resolved), very similar to the 52.8% efficiency of the "default" sample (20.0% from merged + 32.8% from resolved).

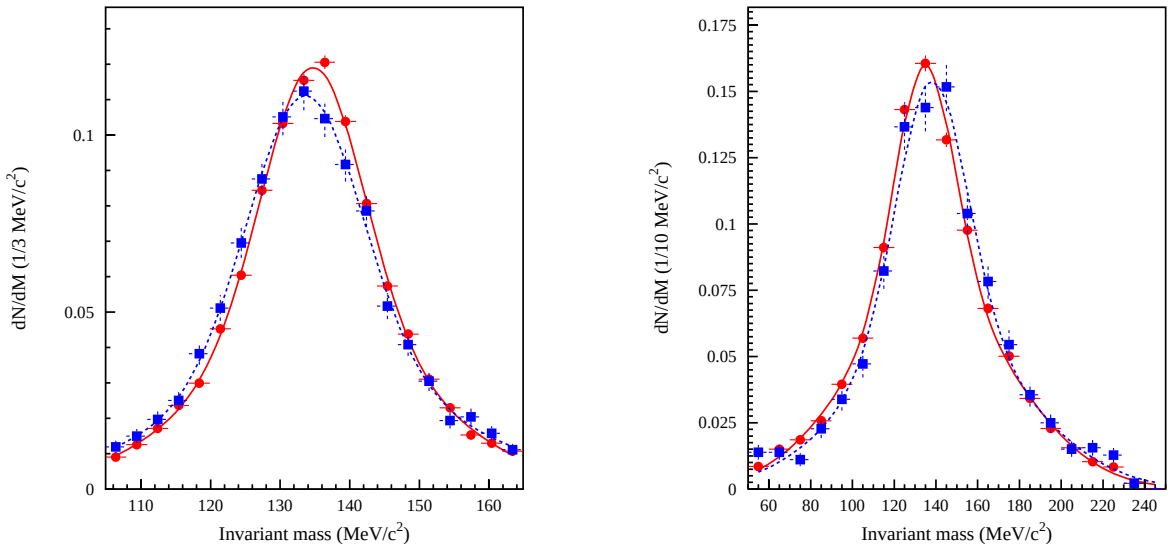

Figure 24: The mass distribution of the π^0 from the $B_d \to \pi^+\pi^-\pi^0$ signal, reconstructed and identified as resolved (left) and merged (right), for the generic sample (red point and solid line) and "robustness test" sample (blue boxes and dashed line). Both distributions are normalized to unity.

The effect of the robustness test on the offline selected $B_d \to \pi^+\pi^-\pi^0$ events (without trigger selection) is detailed in the reference [9]. A global efficiency decrease of $\sim 10\%$ is observed.

Table 3: Parameters of the double gaussian fit of the mass of the resolved and merged π^0 from the $B_d \to \pi^+\pi^-\pi^0$ signal for the default and "robustness test"samples, respectively. .

	parameter		resolved π^0		merged π^0	
			default	robustness	default	robustness
core	height	[%]	7.8± 0.4	8.2±1.7	8.9± 0.3	9.8±1.0
gaussian	peak	[MeV/c^2]	134.7± 0.1	133.6±0.3	134.6± 0.4	138.1±1.3
	sigma	[MeV/c^2]	7.2± 0.2	8.2±1.2	14.1± 0.5	16.7±1.7
2^{nd}	height	[%]	4.1± 0.4	2.9±1.9	7.1± 0.3	5.6±1.0
gaussian	peak	[MeV/c^2]	135.0± 0.2	135.1±1.9	138.2± 0.4	141.7±1.7
	sigma	[MeV/c^2]	16.7± 0.7	21.2±8.5	38.9± 0.6	41.5±2.9

Acknowledgements

We would like to thank members of LHCb Calorimeter team and especially Konstantin Beloous, Vincent Breton, Nicole Brun, Richard Beneyton, Benoit Delcourt and Dmitry Rusinov for their contributions.

It is a great pleasure to thank Profs. Olivier Callot, Roger Forty, Andrey Golutvin and Jacques Lefrancois for numerouse interesting and fruitful discussions.

References

[1] O. Callot, "Calorimeter Data Format and 2D zero suppression scheme", **LHCb-1999-037**

[2] E. Aguilò *et al.*, "Pulseshape simulation and implementation for the Calorimeter system", **LHCb-2003-093**

[3] V. Breton, N. Brun and P. Perret, "A clustering algorithm for the LHCb electromagnetic calorimeter using cellular automaton", **LHCb-2001-123**

[4] H. Terrier and I. Belyaev, "Particle identification with LHCb calorimeters", **LHCb-2003-092**

[5] S. Amato *et al.,* "Reoptimized LHCb Detector Design and Performance", Technical Design Report, **CERN-LHCC-2003-031**

[6] G. Pakhlova and I. Belyaev, "Radiative B-decays at LHCb", **LHCb-2003-090**

[7] F. Teubert, "Study of LHCb Trigger Performance Robustness", **LHCb-2003-059**

[8] R. Hollebeek, "Topics in Calorimetry for High Energy Physics", **1991 SLAC Summer School Lectures**

[9] F. Machefert *et al.*, "$B_d \to \pi^+\pi^-\pi^\circ$ reconstruction", **LHCb-2003-077**

Appendix

A Analytical reconstruction of merged π^0 based on the moments analysis of clusters

The individual impact position and energy of a pair of merged photons can be analytically resolved from the energy distribution of the cluster in the transversal plane
The procedure, based on the energy-weighted moments of the cluster up to the third order, provides correct results assuming the transversal shape of a photon shower is *energy-independant* and *symmetrical*. Experimental effects (incidence angle, shower shape, passive material ...) thus degradates the performance of this analytical method.
The iterative reconstruction of merged clusters pair detailed in the section 2.2 allows to correct the energies and directions from various effects and leads to better performance.
However, the analytical method is faster than the iterative one and could be useful for a rough reconstruction of merged π^0 at the higher levels of trigger, for example. In addition, the moment analysis of cluster could provide useful informations to improve the π^0/γ separation.
The analytical approach based on moments analysis is detailed below.

The n^{th} moment of a cluster is defined as :

$$\langle x^n \rangle = \frac{\sum E_i x_i^n}{\sum E_i}$$

where the sum is looping over all cells owing to the cluster.
For simplification let's rotate the transversal frame (x_0,y_0) into the $\langle x_0 y_0 \rangle$ co-moment eigenframe (x,y) in which by definition the $\langle xy \rangle$ co-moment vanishes. The so defined x-axis is the cluster major-axis. Its rotation angle (φ) with respect to the original frame is given by :

$$\tan 2\varphi = \frac{2\langle x_0 y_0 \rangle}{\langle x_0^2 \rangle - \langle y_0^2 \rangle}$$

Due to the assumed shower symmetry, the two impact points should lies on the major-axis at the unknown positions (x_a,0) and (x_b,0) respectively (see figure 25). In addition, in the (x,y) eigenframe the following four relations occur :

$$\begin{cases} E & = & E_a + E_b & \text{cluster energy} \\ \langle x^1 \rangle & = & \dfrac{x_a E_a + x_b E_b}{E} = 0 & 1^{st} \text{ moment (barycenter) set to zero (origin)} \\ \langle x^2 \rangle & = & \dfrac{x_a^2 E_a + x_b^2 E_b}{E} + \sigma_x^2 & 2^{nd} \text{ moment (variance)} \\ \langle x^3 \rangle & = & \dfrac{x_a^3 E_a + x_b^3 E_b}{E} & 3^{rd} \text{ moment (skewness)} \\ \text{with } \sigma_x^2 & = & \sigma_y^2 = \langle y^2 \rangle & \text{because of the assumed shape symmetry} \end{cases}$$

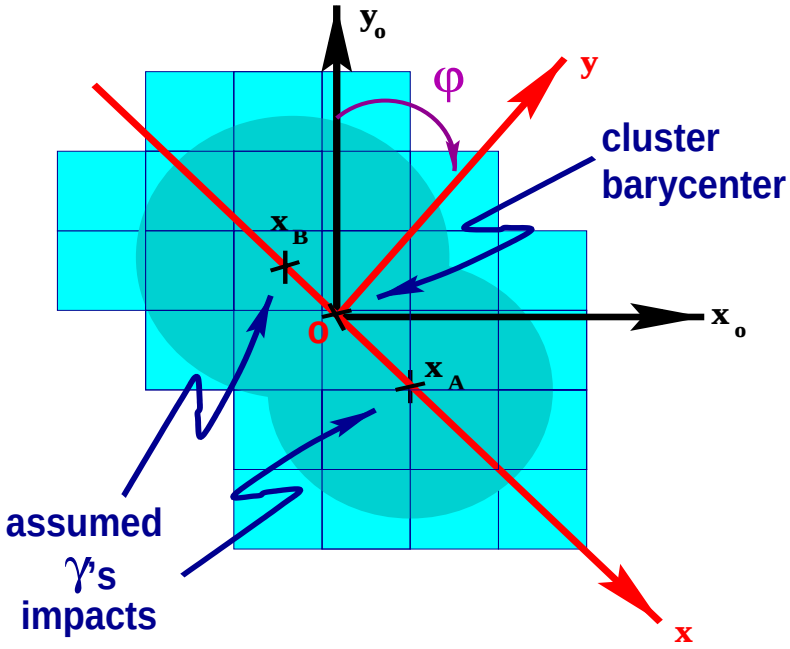

Figure 25: Rotation of the transversal frame to the cluster co-moment eigenframe.

with the four unknowns : E_a, x_a, E_b and x_b, i.e. the energy and the impact position of the two incoming particles, respectively. Without the preliminary frame rotation we would have to handle 8 unknowns (x_a, y_a, E_a, x_b, y_b, E_b, σ_x and $\sigma_y \neq \sigma_x$) and thus to require additional constraints from $\langle y^1 \rangle$, $\langle y^2 \rangle$, $\langle y^3 \rangle$ and $\langle xy \rangle$ (co-)moments to (obviously) obtain the same solution.
Note that the assumed *symmetry* and *energy-independance* of shower are mandatory in order the relations about the variance and the skewness are correct, respectively.

The resolution of the equations system leads to the following solutions :

$$\begin{cases} x_a &= \dfrac{\langle x^3 \rangle \pm \sqrt{\langle x^3 \rangle^2 + 4\left(\langle x^2 \rangle - \langle y^2 \rangle\right)^3}}{2\left(\langle x^2 \rangle - \langle y^2 \rangle\right)} \\ x_b &= \dfrac{-\left(\langle x^2 \rangle - \langle y^2 \rangle\right)}{x_a} \\ E_b &= E\dfrac{x_a}{x_a - x_b} \\ E_a &= E - E_b \end{cases}$$

The sign ambiguity for x_a is meaningless, it just swaps the two solutions labelled a and b and can be choosen arbitrary.

The solution can easily be rotated to the original (x,y) frame with an inverse rotation :

$$\begin{aligned} x_0 &= x\cos\varphi + y\sin\varphi \\ y_0 &= y\cos\varphi - x\sin\varphi \end{aligned}$$

Assuming the two impact points separation is small with respect to the distance to the origin of the particles pair, the invariant mass is simply related to the 2^{nd} moments.
To the first approximation, the invariant mass can be written as :

$$M_{ab}^2 = E_a E_b \left(1 - \cos\Delta\Theta_{ab}\right) \sim E_a E_b \frac{\left(x_a - x_b\right)^2}{r^2}$$

(using $\Delta x_{ab} \sim r\Delta\Theta_{ab}$ and $\cos\Delta\Theta_{ab} \sim 1 - \frac{\Delta\Theta_{ab}^2}{2}$) where r represents the distance between the cluster and the primary vertex ($r_a \sim r_b \sim r$). Using the solutions given above we obtain :

$$\begin{aligned} r^2.M_{ab}^2 &= \left(E - E_b\right)\left(Ex_a\right)\left(x_a - x_b\right) = E^2 x_a\left(x_a - x_b\right) - \left(E.x_a\right)^2 \\ &= -E^2 x_a x_b = E^2\left(\langle x^2\rangle - \langle y^2\rangle\right) \end{aligned}$$

So in the co-moment eigenframe we have :

$$M_{ab}^2 = \frac{E^2}{r^2}\left(\langle x^2\rangle - \langle y^2\rangle\right)$$

which can be expressed as :

$$\boxed{M_{ab}^2 = \frac{E^2}{r^2}\frac{\langle x_o^2\rangle - \langle y_o^2\rangle}{\cos 2\varphi_0}}$$

in any arbitrary frame φ_0-rotated with respect to the co-moment eigenframe.

The figure 26 displays the invariant mass obtained with this analytical method for merged π^0 from $B_d \to \pi^+\pi^-\pi^0$ events. The core resolution of the π^0 peak is $\sim$26 MeV to be compared to $\sim$15 MeV for the iterative method.

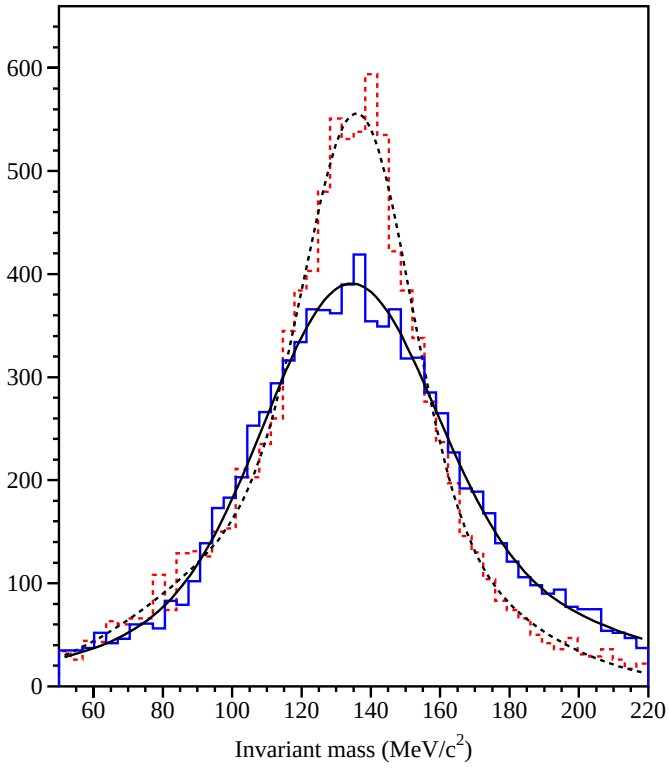

Figure 26: The invariant mass obtained with the analytical reconstruction method based on cluster moments analysis for merged π^0 from $B_d \rightarrow \pi^+\pi^-\pi^0$ events (solid histogram). The iterative method result (dashed histogram) is superimpose for comparison purpose.